Object-Based Spatial Feature for Classification of Very High Resolution Remote Sensing Images

Penglin Zhang, Zhiyong Lv, and Wenzhong Shi

***Abstract*—This letter presents a novel spatial feature called object correlative index (OCI) to enhance the classification of very high resolution images. This novel method considers the property of an image object based on spectral similarity to construct a useful OCI to describe the spatial information objectively. Compared with the generic features widely used in image classification, the classification approach based on the OCI spatial feature results in higher classification accuracy than those approaches that only consider spectral features or pixelwise spatial features, such as the pixel shape index and mathematical morphology profiles. Experiments are conducted on QuickBird satellite image and aerial photo data, and results confirm that the proposed method is feasible and effective.**

***Index Terms*—Classification of very high resolution (VHR) image, object correlative index (OCI), spatial feature, spectral feature.**

I. Introduction

VERY high resolution (VHR) images can provide more detailed information of the Earth surface and have opened up avenues for remote sensing applications. However, the availability of these applications poses challenges to image classification [1]. To overcome these challenges, the classification of VHR images must be complemented by other means [2]. Therefore, some spatial feature extraction methods have been proposed to classify VHR remote sensing images [3]–[5].

Several pixelwise spatial features have been reported. Shackelford and Davis [6] proposed the length–width extraction algorithm (LWEA), a shape spatial feature extraction algorithm for VHR images that can compute the "length and width" of a given central pixel using spectral similarity. LWEA is similar to the gray-level co-occurrence matrix [7], which determines the spectral similarity between a central pixel and its surrounding pixels. Zhang *et al.* [2] proposed an improved LWEA by providing a pixel shape index (PSI) which describes the spatial information around the central pixel, and PSI has been described in a previous study [1]. In addition to the aforementioned methods, mathematical morphology (MP) is useful in the representation and description of regional features which have been successfully applied to urban VHR images [8], [9].

Manuscript received February 26, 2013; revised April 10, 2013; accepted April 30, 2013. Date of publication August 1, 2013; date of current version October 10, 2013. This work was supported by the High Technology Program of China under Grant 2012BAJ15B04.

P. Zhang and Z. Lv are with the School of Remote Sensing and Information Engineering, Wuhan University, Wuhan 430079, China.

W. Z. Shi is with the Joint Spatial Information Research Laboratory between the Hong Kong Polytechnic University and Wuhan University, Wuhan University, Wuhan 430079, China (e-mail: john.wz.shi@polyu.edu.hk).

Color versions of one or more of the figures in this paper are available online at http://ieeexplore.ieee.org.

Digital Object Identifier 10.1109/LGRS.2013.2262132

Compared with the pixelwise approaches, the object-oriented technique is one of the most typical techniques to classify VHR images [10]. Some advantages of object-oriented techniques in VHR imagery have been proved in [11]. This is because pixelwise approaches are often sensitive to noise, which often causes spatial inconsistency and the salt–pepper result [12], [13].

Therefore, this letter proposes an object-based spatial feature, named OCI, for VHR image classification. OCI is an index which describes the correlativity between the central object and its neighboring objects by detecting the spectral similarity. This is used to reveal the potential relationship between a central object and its neighboring objects based on spectral similarity and spatial relationship. The objects will pose similar OCI values when they are located in shape and size homogeneous areas, such as two houses, two farmlands, etc. If an object has a larger OCI value, it has a tighter relationship between the object and its neighbor on spectral similarity; otherwise, it is relaxed. To investigate the robustness of OCI, the neural net algorithm (NN) [14], maximum likelihood classifier (MLC) [15], and support vector machine (SVM) [16], [17] are used as classifiers in this study.

The succeeding sections in this letter are organized as follows. Section II describes the proposed algorithm used to extract OCI. Two experiments are analyzed in Section III: 1) OCI is compared with (a) spectral information only and (b) other pixelwise spatial features, and 2) the parameter sensitivity of the proposed OCI extraction method is evaluated. Section IV discusses the results and provides the conclusion of this study.

II. Methodology

OCI is a spatial feature extracted in an object-by-object manner. In this letter, image objects are extracted using the fractal net evolution approach which is embedded in the eCognition software. The shape-processing filter tool in the eCognition software is used to process the image objects to ensure that they have a convex shape, which confirms that the center of gravity of each image object is inside. The flowchart of the OCI extraction algorithm is shown in Fig. 1, and each image object is scanned and processed by the iterative procedure which is labeled by the dotted rectangle in Fig. 1. In addition, three steps of this extraction method are summarized as follows: 1) Extend the correlative line of the object based on spectral similarity along each direction, 2) measure the distance between "from object" and "to object" in each direction, and 3) calculate the values of OCI features.

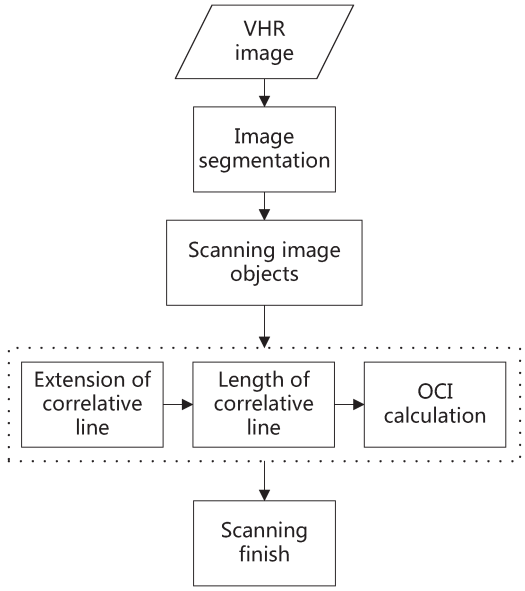

Fig. 1. Flowchart of the proposed OCI extraction method.

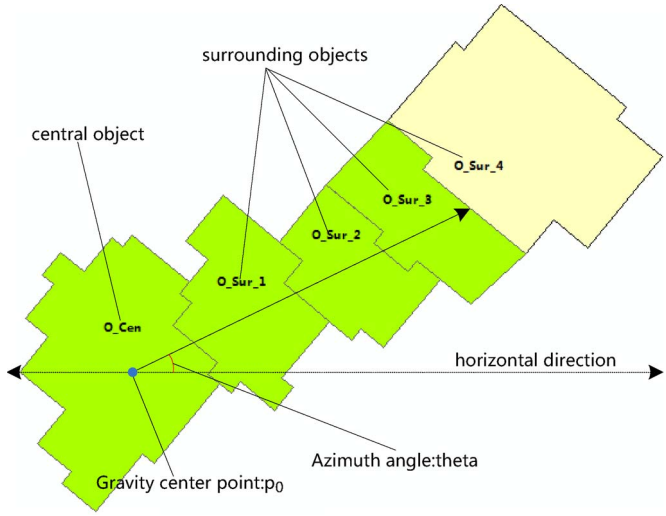

Fig. 2. Extension of the correlative line.

A. Extension of Object Correlative Line

For a specific central object, correlative lines are oriented toward many directions from the center of its gravity; these lines are extended with respect to the spectral similarity of the detected objects (Fig. 2). A correlative line detects the correlative objects by measuring the spectral similarity between the central object and its surrounding objects that spatially intersect the correlative line. In this case, the surrounding objects (i.e., o_Sur_1, o_Sur_2, o_Sur_3, and o_Sur_4 in Fig. 2) are determined whether or not they belong to the same area as the central object (i.e., o_Cen in Fig. 2). In Fig. 2, the blue point indicates the center of gravity (p_0) of the central object and the red arc corresponds to the azimuth angle (θ) that starts from the horizontal line (dotted line with double arrows).

The correlative line along the ith direction can be expressed as

$$y_i = \tan(i \times \theta) \times (x_i - x_0) + y_0 \tag{1}$$

where the gravity center of the central object O^{Cen} is $p_0(x_0, y_0)$, the difference between consecutive azimuth angles is a constant θ, and y_i is the ith correlative line that starts from point p_0. The surrounding objects O^{Sur} are the image objects that spatially intersect y_i. The mean spectral similarity M_i^{sim} between O^{Cen} and O^{Sur} is defined as follows:

$$M_i^{\mathrm{sim}} = |O_s^{\mathrm{cen}} - O_s^{\mathrm{sur}}| \tag{2}$$

where O_s^{cen} and O_s^{sur} represent the mean spectral value of O^{Cen} and O^{Sur}, respectively. The ith correlative line is extended in a stepwise manner considering the following conditions are satisfied, but this extension along the ith direction is terminated if either of these conditions is not met. (1) M_i^{sim} is less than a predefined threshold T_1, and 2) the total number of objects detected by the ith correlative line is less than another predefined threshold T_2.

B. Length of the Correlative Line of the Object

When the ith correlative line extension is terminated, there will be at least one intersection point generated between the line and the polygon of the end image object. The intersection points are assumed as $\{p_1, p_2, p_3, \ldots, p_n\}$; thus, we can determine the apogee point $p_f(x_f, y_f)$ with respect to the gravity center $p_0(x_0, y_0)$. Because some researchers have revealed the advantages of the maximum city-block distance used to describe the spatial feature in VHR images [2], the maximum city-block distance is adopted in this study to measure the length of the correlative line. The length of the ith correlative line is given by

$$d_i = max\left\{|x_0 - x_f|, |y_0 - y_f|\right\} \tag{3}$$

where d_i is the correlative distance from p_0 to p_f.

C. Calculation of OCI Feature

To calculate the value of OCI for a central object, the length can be expressed as $\{d_1, d_2, d_3, \ldots, d_N\}$, where N is the total number of directions and $N = 360/\theta$, with θ as the azimuth angle constant. OCI is defined by the total length of all the directions and expressed as

$$OCI_j^{\mathrm{cen}} = \sum_{i=1}^{N} d_i \tag{4}$$

where OCI_j^{cen} denotes the OCI value of the jth central object. OCI_j^{cen} refers to the correlation between the central object and its surrounding objects based on their spectral similarity.

III. Experiment

In this section, two VHR remote sensing images validate the effectiveness and robustness of the proposed feature for classification. Three parts are designed to achieve the objectives. In the first part, a study area is well described, and in the second part, an experiment is performed to compare the accuracy of different features, such as the PSI, MPs, and spectral feature, with the proposed OCI by using three classifiers: NN, MLC,

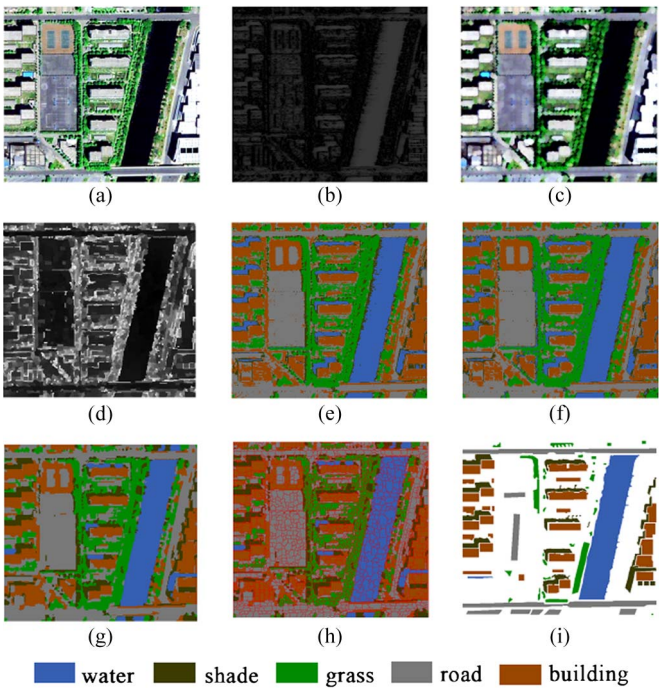

Fig. 3. Results of spectral feature coupled with different spatial features classified by SVM: (a) QuickBird RGB bands (false-color) image; (b) PSI feature image; (c) three feature images generated by MP—open operator; (d) OCI feature image; (e) classification result using PSI feature; (f) classification result using MP feature; (g) classification result using OCI feature; (h) superimposition of the segmental objects on the classification result based on OCI; and (i) ground reference data.

and SVM. Finally, another experiment is designed to test the influence of the parameters based on aerial data.

A. Study Area

To assess the effectiveness and robustness of the proposed spatial feature for classification of VHR remote sensing images, two real remote sensing images are obtained.

The first one is a satellite image of Xuzhou City in the east of China. This satellite image is used in the experiment to test the advantages of the proposed feature for classification. The satellite data are obtained from a QuickBird sensor at a resolution of 0.6 m, as shown in Fig. 3(a). The test image is composed of 416 lines and 375 columns, covering approximately 250 m $\times$ 250 m. This image presents a typical urbanized area in China, which includes five classes: water, shade, grass, road, and building.

The second image, as shown in Fig. 4(a), is acquired by the airborne ADS80 sensor. Here, the relative flying height approximates to 3000 m, and the spatial resolution is 0.32 m. The aerial image is used to analyze the parameter sensitivity of the OCI extraction method for classification. The image is classified into five classes, namely, water, shade, grass, road, and building.

For both data sets, classification becomes challenging because the roads and buildings as well as the waters and shades may be confused with one another and, hence, uncertainties may arise. Each training pixel set and test pixel (Tables I and III) is randomly selected. The training pixel relates to its corresponding object. Take Table I for example: 98/6256 means

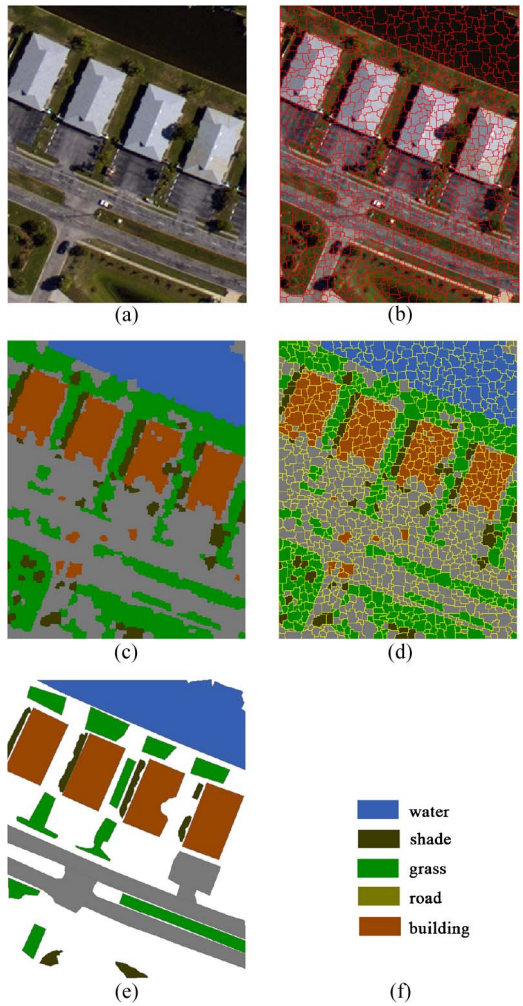

Fig. 4. Result of classification using SVM-based OCI coupled with spectral feature ($\theta = 8$, $T_1 = 30$, and $T_2 = 45$). (a) Aerial data; (b) segmental result; (c) classification result; (d) superimposition of the segmental objects on the classification result of OCI feature; (e) ground reference data; and (f) label of classes.

TABLE I
NUMBER OF TRAINING AND TEST PIXELS FOR QUICKBIRD IMAGE

class	training pixels	test pixels
water	98/6256	17791
shade	43/2727	8831
grass	54/3097	4800
road	66/5826	12048
building	65/6301	16328

6256 training pixels are corresponding with 98 image objects. The available reference data are shown in Figs. 3(h) and 4(h).

B. Experimental Setup and Parameter Settings

To evaluate the accuracy of different features, two experiments are designed in this study. The first experiment is designed as follows.

1) PSI. This feature is extracted according to a previously described algorithm [2], and three parameters are selected ($T1 = 30$, $T2 = 110$, and $D = 22.5$).
2) MP. The image is operated by commonly used operators: erosion and dilation of f by structure element (SE), namely, $\Delta^{\mathrm{SE}}(f)$ and $\nabla^{\mathrm{SE}}(f)$, respectively. In the

TABLE II
PARAMETERS OF OCI FOR TESTING THEIR INFLUENCE ON CLASSIFICATION ACCURACY OF AERIAL DATA

θ	T_1=30 / T_2=45	8	9	10	12	15	18	20	24	30	36
T_1	$\theta = 20$ / T_2=45	8	11	14	17	20	23	26	29	32	35
T_2	$\theta = 20$ / T_1=30	5	10	15	20	25	30	35	40	45	50

TABLE III
NUMBER OF TRAINING AND TEST PIXELS FOR AERIAL DATA

class	training pixels	test pixels
Water	12/1546	15554
shade	7/481	2930
grass	12/1998	10520
road	15/2087	16879
building	16/1782	17441

experiment, the type of the structure is a disk, $SE = 7 \times 7$. Three bands in the original image are operated by close $(\nabla^{\mathrm{SE}}(f) \rightarrow \Delta^{\mathrm{SE}}(f))$ to remove the small right and operated by open $(\Delta^{\mathrm{SE}}(f) \rightarrow \nabla^{\mathrm{SE}}(f))$ to remove dark details. Then, the characteristic image which is used for classification consisted of six new bands and the original three bands.

3) OCI. The proposed feature is extracted by the method detailed in Section II, and some related parameters are set as follows: scale parameter $= 10$, shape parameter $= 0.8$, and compactness $= 0.9$ for segmentation according to a previously described method [18]. The parameters in our proposed algorithm are set at $\theta = 20$, $T_1 = 30$, and $T_2 = 50$.
4) Spectral feature of an object. To prove that the proposed OCI coupled with the spectral feature is helpful for classification, the mean spectral feature of each image object is extracted based on the same segmental parameters as in step 3), and the result of classification is calculated using only the spectral feature of an object.

At the end of each feature extraction, each new feature is considered as a new band fused with the original RGB bands for classification. In particular, OCI is considered as a new characteristic for each image object. Three supervised classifiers are then used in this study to generate the classification map. The parameters of each classifier are set as follows: 1) NN, activation method $=$ logistic, training threshold contribution $= 0.9$, training rate $= 0.2$, training momentum $= 0.9$, number of hidden layers $= 1$, training RMS exit criteria $= 0.1$, and number of training iterations $= 1000.0$; 2) MLC, data scale factor $= 1000.0$; and 3) SVM with RBF kernel function parameters are set by cross-validation.

The second experiment is performed to test the sensitivity of the parameters used in the process of OCI extraction, including azimuth angle (θ), threshold of the mean spectral value (T_1), and threshold of the total number of objects along each direction (T_2). The experimental approach uses one varying parameter, and the other parameters are constant (Table II). The SVM classifier with RBF kernel function and parameters, which is used in this experiment, is set by cross-validation. The training sample and test data are shown in Table III.

TABLE IV
COMPARISONS OF DIFFERENT FEATURES IN DIFFERENT CLASSIFIERS FOR QUICKBIRD IMAGE

classifier / feature	NN		MLC		SVM	
	OA(%)	Ka	OA(%)	Ka	OA(%)	Ka
PSI	79.1414	0.7286	84.6985	0.7989	84.1165	0.7904
MP	80.1515	0.7380	85.1667	0.8052	85.1216	0.8038
OCI	92.4781	0.9021	91.1152	0.8841	90.8469	0.8805
spectral feature only	88.6129	0.8513	86.7945	0.8275	86.6256	0.8251

C. Experimental Results

In the two experiments, the proposed OCI is compared with only PSI, MP, and spectral feature only of objects based on three classical classifiers (NN, MLC, and SVM). The sensitivity of the parameters of the OCI extraction algorithm is verified using SVM. The following results are obtained.

1) Comparison of PSI, spatial features of MP, and spectral feature. The results are enhanced when the proposed OCI spatial feature coupled with the spectral feature is used for classification compared with the results when we used the PSI coupled with the spectral feature, the MP coupled with the spectral feature, and the spectral feature only. Based on the parameter setting in Section III-B, we calculated the overall accuracy (OA) and kappa coefficient (Ka) from the corresponding confused matrix of each classifier (Table IV). OCI improves the accuracy in each classifier. The image of PSI, the classification map using PSI, and the classification map using the OCI feature and SVM are shown in Fig. 3(b), (e), (g), respectively. The image of MP is shown in Fig. 3(c), in which PSI and MP cannot achieve a satisfactory classification particularly for some similar spectral classes such as shade and water. PSI and MP also exhibit more noise than OCI in their classification maps. To prove this advantage of OCI, we calculated the accuracy of classification by using only the spectral features of objects (Table IV). OA and Ka are similarly improved when OCI is used.
2) Robustness of OCI based on different classifiers: Three different classifiers, namely, NN, MLC, and SVM, are used to test the robustness of the OCI feature for classification. Table IV shows that the proposed OCI coupled with spectral information can obtain higher accuracy for each classifier. The OA of OCI is more than 90%, and Ka reaches 0.88, which is higher than that of PSI, MP, or the spectral feature only of the corresponding classifier.
3) Sensitivity of parameters in the process of OCI extraction. The data used for this experiment are shown in Fig. 4(a). Some classification results and ground reference data are illustrated in Fig. 4. To test the sensitivity of the three parameters (θ, T_1, and T_2) in the extraction algorithm, varying parameters (Table II) are used in this study. This test indicates that θ is a parameter representing the capability of OCI to describe a relationship. The accuracies of classification with different θ values are shown in Fig. 5(a) and (b). T_1 indicates the maximum spectral difference between the central object and its surrounding object along each direction. T_1 should be adjusted in accordance with different images. For an aerial image, the

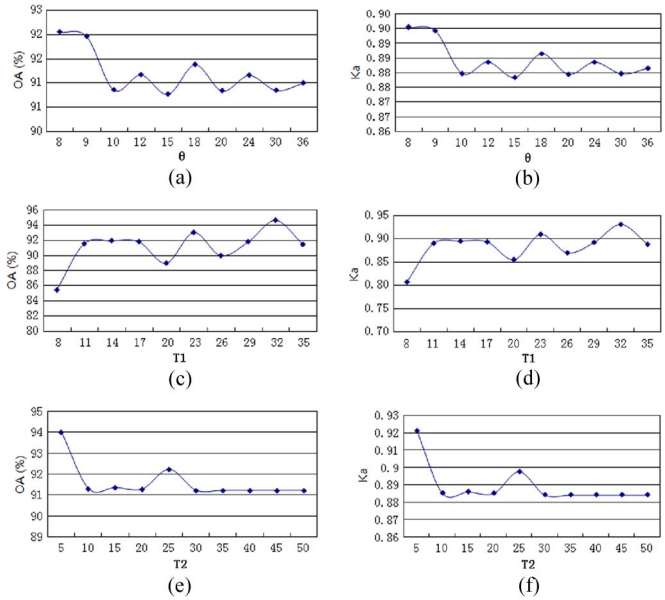

Fig. 5. Analysis of parameter sensitivity in OCI-based classification for aerial data.

classification accuracies increase as T_1 increases from 8 to 11 and the accuracies remain almost similar when T_1 ranges from 8 to 35 [Fig. 5(c) and (d)]. T_2 indicates the maximum number of related objects in the spectral mean along each direction. The relationship among OA, Ka, and T_2 are shown in Fig. 5(e) and (f).

IV. Discussion and Conclusion

In this letter, a novel spatial feature called OCI has been proposed for VHR image classification. OCI can effectively describe the image–object relationship based on spectral similarity according to a simple extended algorithm. The proposed OCI leads a notable increase of classification accuracy as compared with other spatial features while they are both combined with spectral information. The results of using spectral features complemented by OCI and without OCI were also analyzed. A simple extended algorithm has been designed to extract OCI. A correlative line is extended based on the angle and spectral similarity. The correlative length in one direction is defined by the distance from the center of gravity to the apogee intersection point. Three parameters of the OCI extraction algorithm were also calibrated in our experiment.

The accuracies between different features and classifiers were compared. The result of our experiment indicates that OCI can be used to achieve accurate classification, which is indicated by an evident improvement in the accuracy of OA and Ka. Our experiment also reveals that the proposed OCI coupled with spectral information can be used to enhance the classification of VHR remote sensing images by using NN, MLC, and SVM. The proposed OCI feature in this study is very simple, and its reliability should be further evaluated. We recommend that the definition of this feature be improved in future studies.

Acknowledgment

The authors would like to thank the Editor and referees for their helpful suggestions.

References

[1] X. Huang, L. Zhang, and P. Li, "Classification and extraction of spatial features in urban areas using high-resolution multispectral imagery," *IEEE Geosci. Remote Sens. Lett.*, vol. 4, no. 2, pp. 260–264, Apr. 2007.

[2] L. Zhang, X. Huang, B. Huang, and P. Li, "A pixel shape index coupled with spectral information for classification of high spatial resolution remotely sensed imagery," *IEEE Trans. Geosci. Remote Sens.*, vol. 44, no. 10, pp. 2950–2961, Oct. 2006.

[3] F. Dell'Acqua, P. Gamba, A. Ferrari, J. A. Palmason, J. A. Benediktsson, and K. Arnason, "Exploiting spectral and spatial information in hyperspectral urban data with high resolution," *IEEE Geosci. Remote Sens. Lett.*, vol. 1, no. 4, pp. 322–326, Oct. 2004.

[4] M. Fauvel, J. A. Benediktsson, J. Chanussot, and J. R. Sveinsson, "Spectral and spatial classification of hyperspectral data using SVMs and morphological profiles," *IEEE Trans. Geosci. Remote Sens.*, vol. 46, no. 11, pp. 3804–3814, Nov. 2008.

[5] Y. O. Ouma, J. Tetuko, and R. Tateishi, "Analysis of co-occurrence and discrete wavelet transform textures for differentiation of forest and non-forest vegetation in very-high-resolution optical-sensor imagery," *Int. J. Remote Sens.*, vol. 29, no. 12, pp. 3417–3456, Jun. 2008.

[6] A. K. Shackelford and C. H. Davis, "A hierarchical fuzzy classification approach for high-resolution multispectral data over urban areas," *IEEE Trans. Geosci. Remote Sens.*, vol. 41, no. 9, pp. 1920–1932, Sep. 2003.

[7] F. Agüera, F. J. Aguilar, and M. A. Aguilar, "Using texture analysis to improve per-pixel classification of very high resolution images for mapping plastic greenhouses," *ISPRS J. Photogramm. Remote Sens.*, vol. 63, no. 6, pp. 635–646, Nov. 2008.

[8] R. Bellens, S. Gautama, L. Martinez-Fonte, W. Philips, J. C.-W. Chan, and F. Canters, "Improved classification of VHR images of urban areas using directional morphological profiles," *IEEE Trans. Geosci. Remote Sens.*, vol. 46, no. 10, pp. 2803–2813, Oct. 2008.

[9] M. Pesaresi and J. A. Benediktsson, "A new approach for the morphological segmentation of high-resolution satellite imagery," *IEEE Trans. Geosci. Remote Sens.*, vol. 39, no. 2, pp. 309–320, Feb. 2001.

[10] Y. Tang, L. Zhang, and X. Huang, "Object-oriented change detection based on the Kolmogorov–Smirnov test using high-resolution multispectral imagery," *Int. J. Remote Sens.*, vol. 32, no. 20, pp. 5719–5740, Oct. 2011.

[11] E. Pagot, M. Pesaresi, D. Buda, and D. Ehrlich, "Development of an object-oriented classification model using very high resolution satellite imagery for monitoring diamond mining activity," *Int. J. Remote Sens.*, vol. 29, no. 2, pp. 499–512, Jan. 2008.

[12] P. Soille, *Morphological Image Analysis: Principles and Applications*. New York, NY, USA: Springer-Verlag, 2003.

[13] X. Huang and L. Zhang, "An adaptive mean-shift analysis approach for object extraction and classification from urban hyperspectral imagery," *IEEE Trans. Geosci. Remote Sens.*, vol. 46, no. 12, pp. 4173–4185, Dec. 2008.

[14] M. Chini, F. Pacifici, W. J. Emery, N. Pierdicca, and F. Del Frate, "Comparing statistical and neural network methods applied to very high resolution satellite images showing changes in man-made structures at rocky flats," *IEEE Trans. Geosci. Remote Sens.*, vol. 46, no. 6, pp. 1812–1821, Jun. 2008.

[15] J. D. Paola and R. A. Schowengerdt, "A detailed comparison of backpropagation neural network and maximum-likelihood classifiers for urban land use classification," *IEEE Trans. Geosci. Remote Sens.*, vol. 33, no. 4, pp. 981–996, Jul. 1995.

[16] M. Volpi, D. Tuia, F. Bovolo, M. Kanevski, and L. Bruzzone, "Supervised change detection in VHR images using contextual information and support vector machines," *Int. J. Appl. Earth Observ. Geoinf.*, vol. 20, pp. 77–85, Feb. 2013.

[17] D. Tuia, F. Pacifici, M. Kanevski, and W. J. Emery, "Classification of very high spatial resolution imagery using mathematical morphology and support vector machines," *IEEE Trans. Geosci. Remote Sens.*, vol. 47, no. 11, pp. 3866–3879, Nov. 2009.

[18] M. Cao, G. Liu, and X. Zhang, "An object-oriented approach to map wetland vegetation: A case study of yellow river delta," in *Proc. IEEE IGARSS*, 2007, pp. 4585–4587.